Electronic Supplementary Information (ESI)

A "Belt" Strategy for Promoting the 3D Network Packing of Fully Non-fused Ring Acceptor in Organic Solar Cells

Tianqiang Cui,‡[a] Zhan Huang,‡[a] Yamin Zhang,*[a] Xiao-Peng Ru,[a] Xingqi Bi,[b] Yun-Tao Ding,[a] Yongrui Yang,[c] Junpeng Dai,[d] Guanghao Lu,[d] Zitong Liu,[a] Yongsheng Chen,*[b] and Hao-Li Zhang*[a]

[a] *State Key Laboratory of Applied Organic Chemistry (SKLAOC), Key Laboratory of Special Function Materials and Structure Design (MOE), College of Chemistry and Chemical Engineering, Lanzhou University, Lanzhou 730000, China.*
E-mail: haoli.zhang@lzu.edu.cn; E-mail: zym@lzu.edu.cn.
[b] *State Key Laboratory and Institute of Elemento-Organic Chemistry, The Centre of Nanoscale Science and Technology and Key Laboratory of Functional Polymer Materials, Renewable Energy Conversion and Storage Center (RECAST), College of Chemistry, Nankai University, Tianjin 300071, China.*
E-mail: yschen99@nankai.edu.cn.
[c] *CAS Key Laboratory of Green Printing, Beijing National Laboratory for Molecular Science (BNLMS), Institute of Chemistry, Chinese Academy of Sciences, Beijing, 100190, China, University of Chinese Academy of Sciences, Beijing 100049, China.*
[d] *Frontier Institute of Science and Technology, Xi'an Jiaotong University, Xi'an 710054, China.*

Table of Contents

1. Materials and Synthesis

All reagents and solvents were purchased from commercial sources and used without further purification.

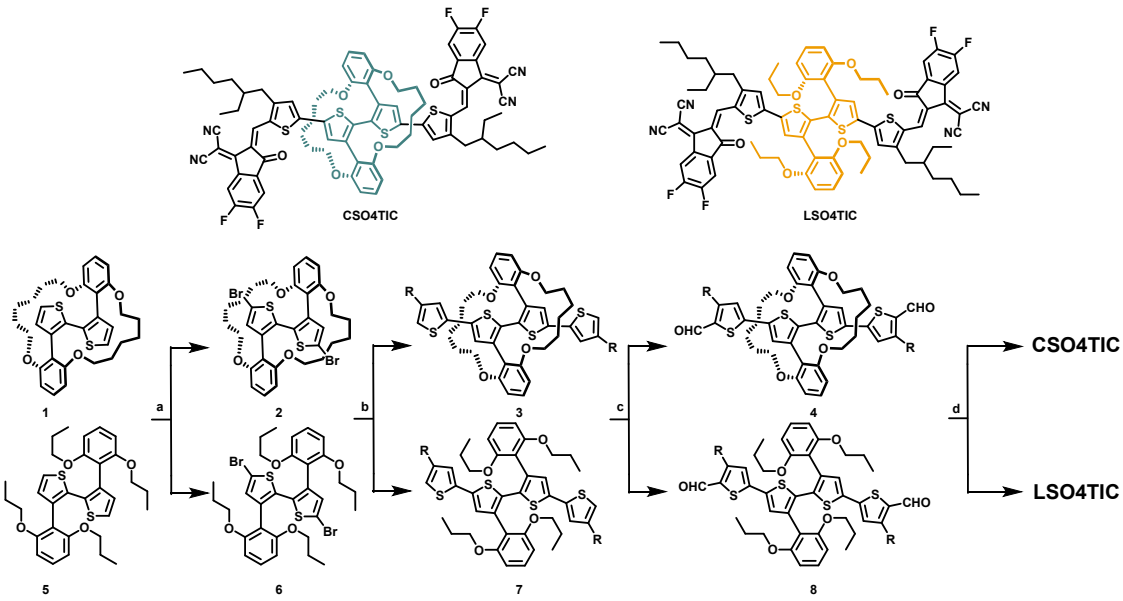

Scheme S1. The synthetic route of CSO4TIC and LSO4TIC. Conditions and reagents: **a)** NBS, AcOH, 0°C; **b)** tributyl(4-(2-ethylhexyl)thiophen-2-yl)stannane, $Pd(PPh_3)_4$, toluene; **c)** DMF, $POCl_3$, $ClCH_2CH_2Cl$; **d)** 2-(5,6-difluoro-3-oxo-2,3-dihydro-1H-inden-1-ylidene)malononitrile, pyridine, $CHCl_3$, RT.

Synthesis of Compound 2 and Compound 6:

Compound 1 was synthesized according to the previous literature, and the single crystal structure was consistent with that reported in the literature.[1] ^{1}H NMR (400 MHz, Chloroform-*d*) δ 7.38 (t, *J* = 8.3, 8.3 Hz, 2H), 6.98 (d, *J* = 5.1 Hz, 2H), 6.75 (d, *J* = 5.1 Hz, 2H), 6.69 (d, *J* = 8.3 Hz, 4H), 4.05 (m, 4H), 3.79 – 3.71 (m, 4H), 1.48 (m, 8H), 1.21 – 1.12 (m, 4H), 0.92 (m, 4H).

To a flame-dried flask were added Compounds 1 (100 mg, 0.183 mmol) and AcOH/ $CHCl_3$ (5 mL/ 10 mL). The solution was allowed to stir at 0°C for 10 min, and then N-bromosuccinamide (2 equiv, 66 mg, 0.37 mmol) was added in one portion and allowed to stir at room temperature. After 2 h, the reaction mixture was poured into

water (100 mL), and the mixture was extracted with CH_2Cl_2 (50 mL × 2). The organic phases were washed with water (100 mL) and dried with Na_2SO_4, and the solvent was removed under reduced pressure. The crude product is not purified for the next step.

Compound 6 was synthesized using the similar synthetic procedure with Compound 2 from Compound 5. ^{1}H NMR (400 MHz, Chloroform-*d*) δ 7.08 – 7.04 (m, 4H), 6.79 (d, *J* = 5.2 Hz, 2H), 6.33 (d, *J* = 8.3 Hz, 4H), 3.67 – 3.60 (m, 8H), 1.53 (m, 10H), 0.80 (t, *J* = 7.4, 7.4 Hz, 12H).

Synthesis of Compound 3 and Compound 7:

Compounds 2 (0.183 mmol), tributyl(4-octylthiophen-2-yl) stannane (270 mg, 0.55 mmol), and Pd $(PPh_3)_4$ (40 mg, 0.035 mmol) were dissolved in anhydrous toluene (10.0 mL) and heated to 110°C under N_2 for 12 h. After being cooled to room temperature, 50 mL of 2 mol/ L KF solution was added and then the resulting mixture continued stirring for 20 min. After being filtered, the filtrate was treated with water and extracted with CH_2Cl_2. The organic layer was collected and dried with anhydrous sodium sulfate, the residual solvent was removed under reduced pressure, and the residue was purified by silica gel chromatography with n-hexane to n-hexane/ dichloromethane (5:1) eluent. Yield = 103 mg, 60%. ^{1}H NMR (400 MHz, Chloroform-*d*) δ 7.40 (t, *J* = 8.3, 8.3 Hz, 2H), 6.87 (s, 2H), 6.73 (s, 2H), 6.70 (d, *J* = 8.3 Hz, 4H), 6.67 (s, 2H), 4.09 (m, 4H), 3.77 (m, 4H), 2.47 (d, *J* = 6.7 Hz, 4H), 1.64 – 1.47 (m, 10H), 1.28 – 1.25 (m, 20H), 1.02 (m, 4H), 0.91 – 0.86 (m, 12H).

Compound 7 was synthesized using the similar synthetic procedure with Compound 3 from Compound 2. ^{1}H NMR (400 MHz, Chloroform-*d*) δ 7.00 (t, *J* = 8.3, 8.3 Hz, 2H), 6.93 (s, 2H), 6.88 (s, 2H), 6.70 (s, 2H), 6.27 (d, *J* = 8.4 Hz, 4H), 3.64 (m, 8H), 2.50 (d, *J* = 6.8 Hz, 4H), 1.59 (*m*, 10H), 1.30 (m, 16H), 0.90 – 0.81 (m, 24H).

Synthesis of Compound 4 and Compound 8:

To a 100 mL two-necked flask, DMF (0.2 mL) and $POCl_3$ (0.15 mL, 1.6 mmol) were added in 30 mL 1,2-dichloroethane (DCE) at 0°C under nitrogen atmosphere. After being stirred at 0°C for 20 min, compound 3 (100 mg, 0.11 mmol) was directly injected into the flask. Then the mixture was stirred at room temperature for 24h. After that, CH_3COONa aqueous solution was added and then the resulting mixture continued

stirring for 60 min. Then the mixture was poured into water and extracted with CH_2Cl_2 three times. The organic layer was washed with water and then dried over $MgSO_4$. After the removal of the solvent, the crude product was purified on a silica-gel column chromatography with dichloromethane as the eluent to afford an orange solid (82 mg, 75%). ^{1}H NMR (400 MHz, Chloroform-*d*) δ 9.92 (s, 2H), 7.46 (t, *J* = 8.3, 8.3 Hz, 2H), 7.10 (s, 2H), 6.86 (s, 2H), 6.71 (d, *J* = 8.4 Hz, 4H), 4.12 (m, 4H), 3.74 (m, 4H), 2.79 (d, *J* = 7.1 Hz, 4H), 1.62– 1.44 (m, 10H), 1.30 (m, 20H), 1.02 – 0.94 (m, 4H), 0.90 (t, *J* = 7.3, 7.3 Hz, 12H).

Compound 8 was synthesized using the similar synthetic procedure with Compound 4. ^{1}H NMR (400 MHz, Chloroform-*d*) δ 9.94 (s, 2H), 7.14 (s, 2H), 7.08 (t, *J* = 8.3, 8.3 Hz, 2H), 6.92 (s, 2H), 6.33 (d, *J* = 8.4 Hz, 4H), 3.68 (m, 8H), 2.82 (d, *J* = 7.2 Hz, 4H), 1.63 - 1.52 (m, 10H), 1.35 – 1.26 (m, 16H), 0.92 – 0.87 (m, 12H), 0.81 (t, *J* = 7.4, 7.4 Hz, 12H).

Synthesis of CSO4TIC and LSO4TIC:

2-(5,6-difluoro-3-oxo-2,3-dihydro-1H-inden-1-ylidene) malononitrile (47 mg, 0.204 mmol) was added to a solution of compound 4 (81 mg, 0.08 mmol) in $CHCl_3$ (15 mL) under nitrogen atmosphere. Then 0.5 mL pyridine was injected into the solution. The mixture was stirred at 40°C for 24 h. After being cooled to room temperature, the mixture was poured into methanol and filtered, then the solid was washed by methanol, and the crude product was purified on a silica-gel column chromatography using n-hexane/ $CHCl_3$ (1:1) as the eluent. **CSO4TIC** was obtained as a deep brown solid (79 mg, 70%). ^{1}H NMR (600 MHz, Chloroform-*d*) δ 8.91 (s, 2H), 8.53 (dd, *J* = 10.0, 6.4 Hz, 2H), 7.66 (t, *J* = 7.5, 7.5 Hz, 2H), 7.54 (t, *J* = 8.4, 8.4 Hz, 2H), 7.40 (s, 2H), 6.93 (s, 2H), 6.76 (d, *J* = 8.4 Hz, 4H), 4.15 (m, 4H), 3.75 (t, *J* = 9.3, 9.3 Hz, 4H), 2.86 (d, *J* = 7.3 Hz, 4H), 1.65 (m, 2H), 1.62 – 1.51 (m, 8H), 1.39 – 1.21 (m, 20H), 1.01 – 0.95 (m, 4H), 0.94 – 0.88 (m, 12H). MOLDI-TOF m/ z: calcd [M^+] for $C_{82}H_{74}F_4N_4O_6S_4$ 1414.4427, found 1414.897.

LSO4TIC was synthesized using the similar synthetic procedure to **CSO4TIC**. ^{1}H NMR (600 MHz, Chloroform-*d*) δ 8.95 (s, 2H), 8.53 (dd, *J* = 10.0, 6.4 Hz, 2H), 7.65 (t, *J* = 7.5, 7.5 Hz, 2H), 7.43 (s, 2H), 7.14 (t, *J* = 8.4, 8.4 Hz, 2H), 7.09 (s, 2H), 6.38 (d,

J = 8.4 Hz, 4H), 3.77 – 3.67 (m, 8H), 2.89 (d, J = 7.4 Hz, 4H), 1.68 (m, 2H), 1.59 (m, 8H), 1.42 – 1.25 (m, 16H), 0.92 – 0.88 (m, 12H), 0.84 (t, J = 7.4, 7.4 Hz, 12H). MOLDI-TOF m/ z: calcd [M^+] for $C_{82}H_{78}F_4N_4O_6S_4$ 1418.4740, found 1418.928.

Single-crystal Growth

Single crystals of CSO4TIC were grown by the vapor diffusion method at room temperature. In detail, A solution prepared from ~2 mg CSO4TIC in ~0.5 mL $CHCl_3$ was transferred into a 5 mL vial. And then, the 5 mL vial was placed in a 20 mL vial containing ~5 mL methanol. The 20 mL vial was then tightly sealed, and left standing for 5-7 days to give rod-shaped crystals. The X-ray diffraction signals of single crystal were collected on Rigaku XtalAB PRO MM007 DW. The crystal was kept at 193.0 K during data collection. The single crystal growth method of LSO4TIC is the same as CSO4TIC.

2. Instruments and Measurements

^{1}H NMR spectra were measured in $CDCl_3$ on Bruker Ultrashield 400 Plus spectrometer. UV-Vis-NIR absorption spectra were taken from a Shimadzu UV-2600 UV-Vis spectrophotometer. The optical bandgaps (E_g^{opt}) were calculated from the onset absorption peak of thin films, using the equation E_g^{opt}=1240/ λ_{edge} (eV). The electrochemical cyclic voltammetry (CV) was performed on a CHI660b electrochemical workstation. All CV measurements were carried at room temperature with a conventional three-electrode configuration with glassy carbon as the working electrode, Ag/ AgCl as the reference electrode, and Pt sheet as the counter electrode, respectively. Anhydrous acetonitrile was used as the solvent. Tetrabutylammonium phosphorus hexafluoride (Bu_4NPF_6) was used as the supplementary electrolyte, and the scan rate was 50 mV s^{-1}. The lowest unoccupied molecular orbital (LUMO) and highest occupied molecular orbital (HOMO) energy levels were calculated from the onset of reduction and oxidation potential, using the equation $E_{LUMO} = -(E_{red,onset} - E_{Fc/Fc+} + 4.8)$ eV and $E_{HOMO} = -(E_{ox,onset} - E_{Fc/Fc^+} + 4.8)$ eV, respectively. The structure optimization and relaxed potential surface energy scans were performed by density functional theory (DFT) calculations utilizing Gaussian 09 at B3LYP/ 6-31G (d, p) level. The 2-

ethylhexyl was replaced by methyl to simplify the calculation. The atomic force microscopy (AFM) images were obtained from Bruker NanoScope V atomic force microscope. The steady-state photoluminescent spectra and photoluminescence quantum yield (PLQY) values were all recorded on the Steady/Transient State Fluorescence Spectrometer (FLS 1000, Edinburgh Instruments, UK).

3. Device Fabrication and Characterization

The devices were fabricated with the configuration of ITO/ PEDOT: PSS/ PBDB-T/ Acceptors/ PDINO/ Ag. The conductive ITO glass substrate was ultrasonically cleaned with ethanol and isopropanol for 15 min each, then treated with UV-ozone for 20 min after fully dried. Secondly, we spin-coated the 0.45 μm-filtered aqueous solution of PEDOT: PSS on the aforementioned ITO substrate at 4500 rpm for 20 s, followed by heating the ITO substrate at 150°C for 20 min and transferring it to a nitrogen-filled glove box. Thirdly, the chlorobenzene solution of PBDB-T was spin-coated onto the cooled ITO/ PEDOT: PSS substrate at 1500 rpm. Subsequently, the prepared acceptor solution was spin-coated onto the donor film and then thermally annealed at 120°C for 5 min. Specifically, the CSO4TIC was dissolved in chloroform in a concentration of 6.0 mg/ mL, together with DBCl (1,3-dibromo-5-chlorobenzene) as an additive, and the concentration of DBCl was 10 mg/ mL; the LSO4TIC was prepared similar to CSO4TIC expect for 2-IN (2-iodonaphthalene) as the additive. Eventually, after cooling to room temperature, 1 mg/ mL of PDINO in methanol was spin-coated on the ITO/ PEDOT: PSS/ PBDB-T/ Acceptors substrates, and then the substrates were placed in a vacuum chamber. When the pressure was less than 4.2×10^{-4} Pa, 60 nm Ag was thermal deposited to complete the device fabrication. The photovoltaic areas of the devices were about 4.00 mm^2.

The current density-voltage (*J-V*) curves of photovoltaic devices were obtained by a Keithley 2400 source-measure unit. The photocurrent was measured under illumination simulated 1000 W m^{-2} AM 1.5G irradiation using a SAN-EI XES-50S2 solar simulator, calibrated with a standard Si solar cell. External quantum efficiencies (EQE) were measured using a lock-in amplifier (SR810, Stanford Research Systems).

The devices were illuminated by monochromatic light from a 150 W xenon lamp passing through an optical chopper and a monochromator. Photon flux was determined by a calibrated standard silicon photodiode.

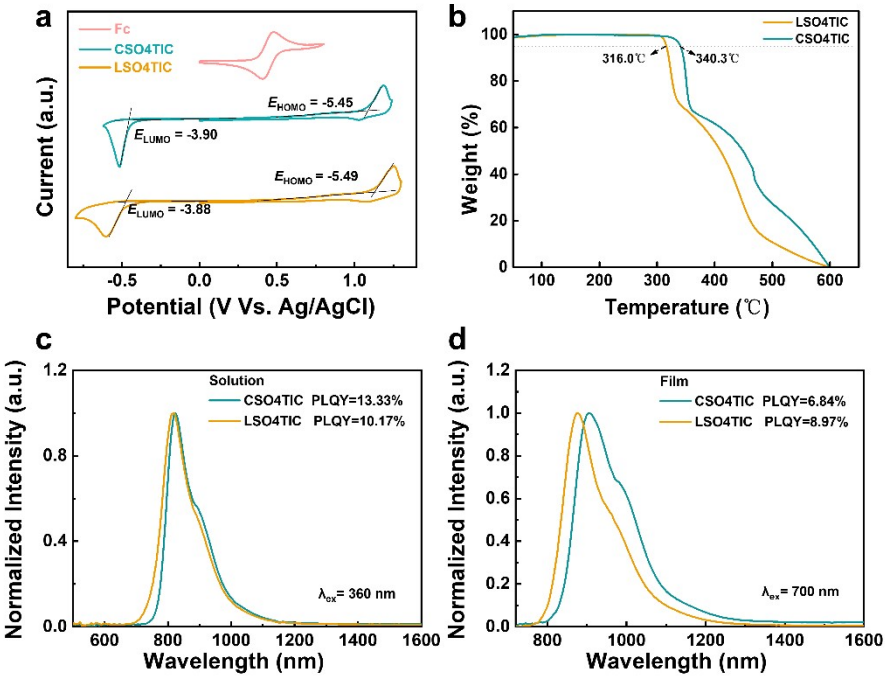

Figure S1. a) Cyclic voltammograms; **b)** Thermogravimetric analysis diagram of CSO4TIC and LSO4TIC; Normalized PL spectra of CSO4TIC and LSO4TIC in c) dilute CF solution and d) film state.

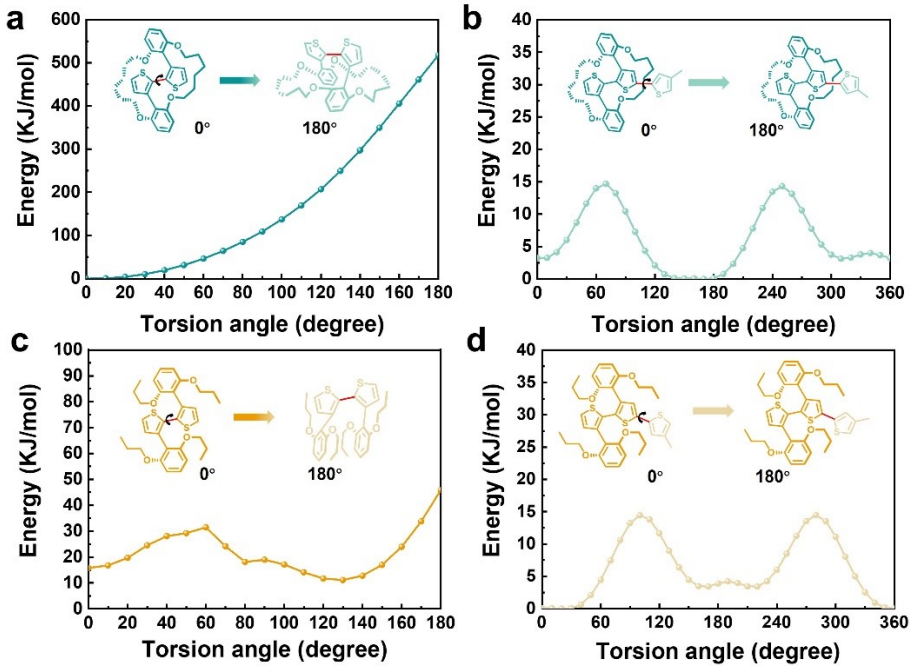

Figure S2. a, c) Rotamers and their energy-torsion angles (*E*-*θ*) curves of **a, c)** the central bithiophenes and **b, d)** the thiophenes in the core and its adjacent thiophenes.

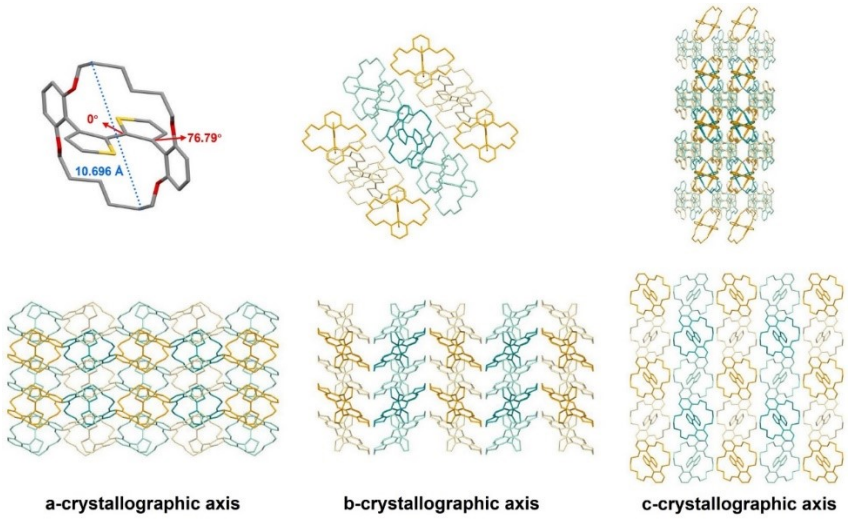

Figure S3. Single-crystal structure and packing mode of bithiophenes connected with the cyclic side chain.

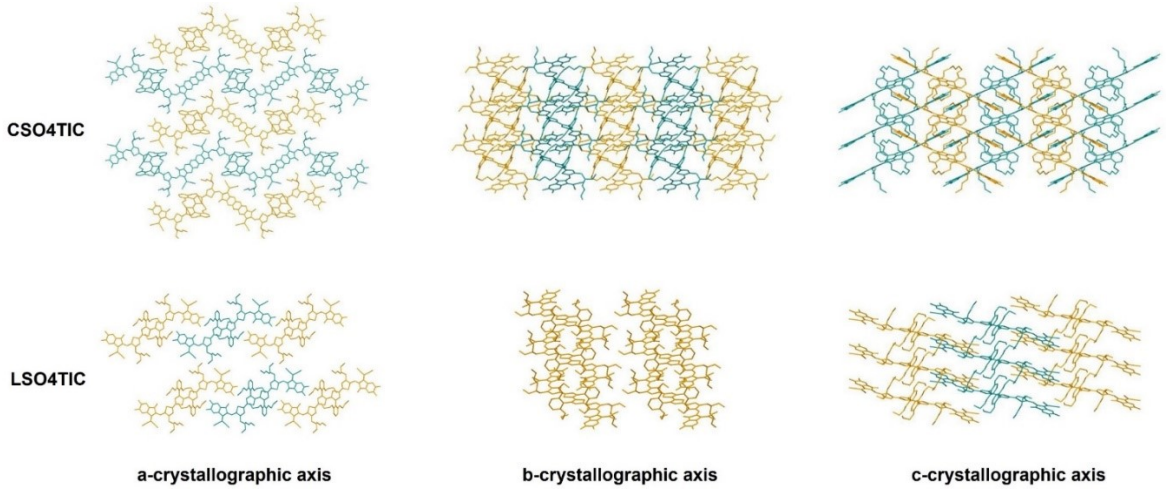

Figure S4. Molecular packing of CSO4TIC and LSO4TIC along a, b and c-crystallographic axis.

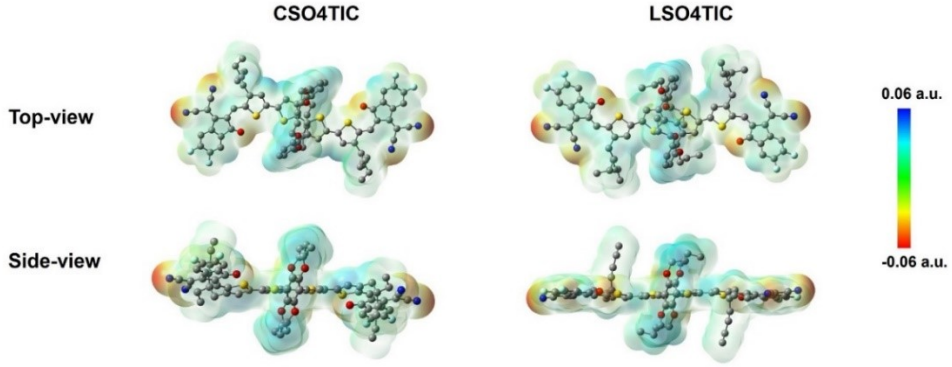

Figure S5. ESP distributions for CSO4TIC and LSO4TIC.

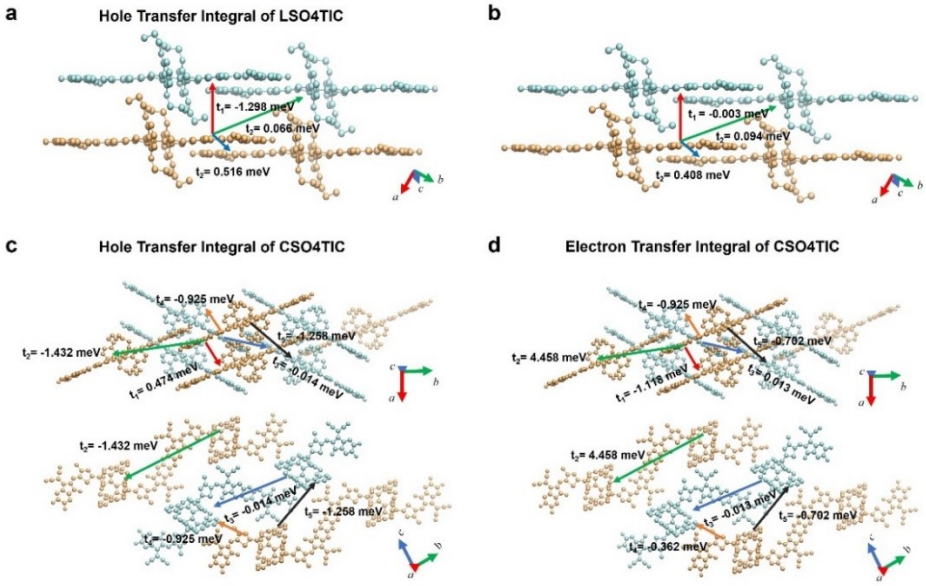

Figure S6. Hole transfer integal and electron transfer integal of CSO4TIC and LSO4TIC.

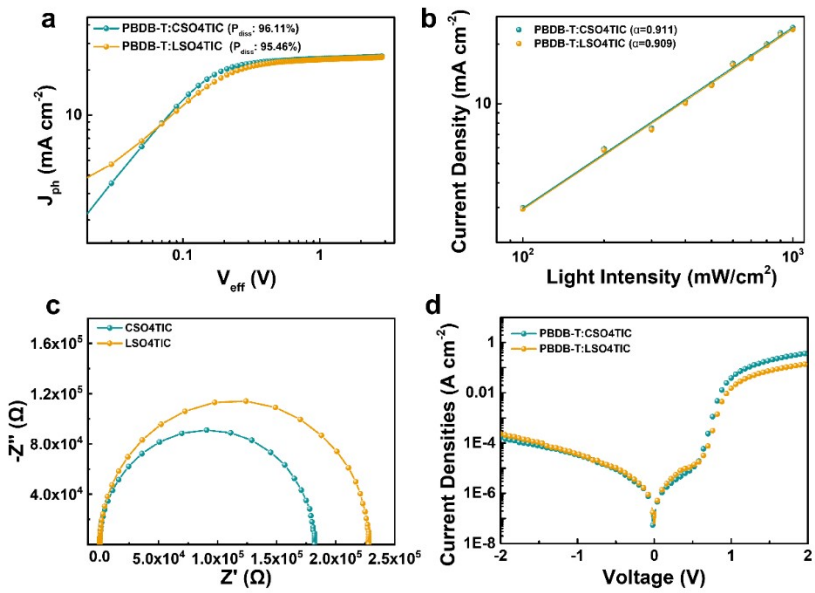

Figure S7. a) Photocurrent density versus effective voltage (J_{ph}-V_{eff}) characteristics for the devices based on PBDB-T/ CSO4TIC and PBDB-T/ LSO4TIC under constant incident light intensity (AM 1.5G, 100 mW cm^{-2}); **b)** Light-intensity dependence of J_{ph} of devices based on PBDB-T/ CSO4TIC and PBDB-T/ LSO4TIC; **c)** Nyquist curves of devices based on PBDB-T/ CSO4TIC and PBDB-T/ LSO4TIC; **d)** J_D–V curves of devices based on PBDB-T/ CSO4TIC and PBDB-T/ LSO4TIC.

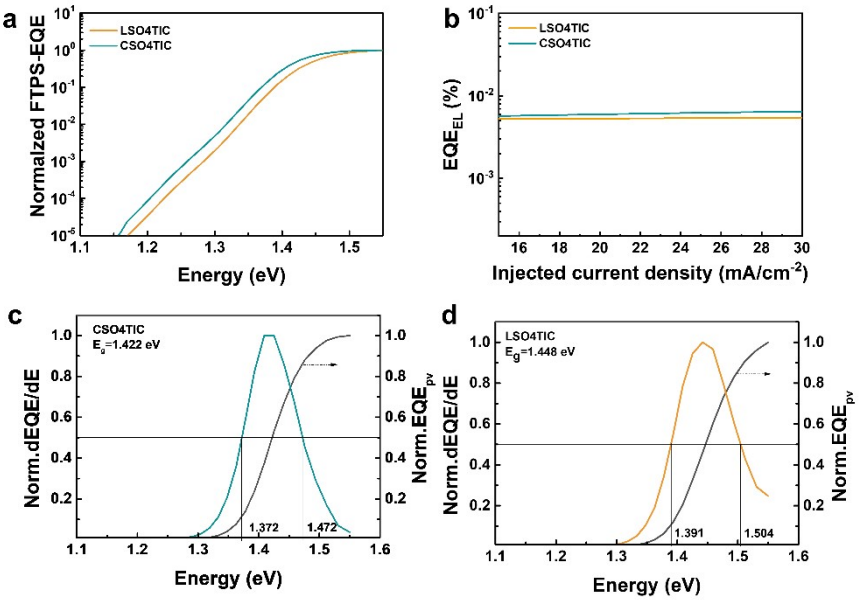

Figure S8. a) The FTPS-EQE and **b)** EQE_{EL} of devices based on PBDB-T/ CSO4TIC and PBDB-T/ LSO4TIC; **c-d)** The band gaps of CSO4TIC and LSO4TIC.

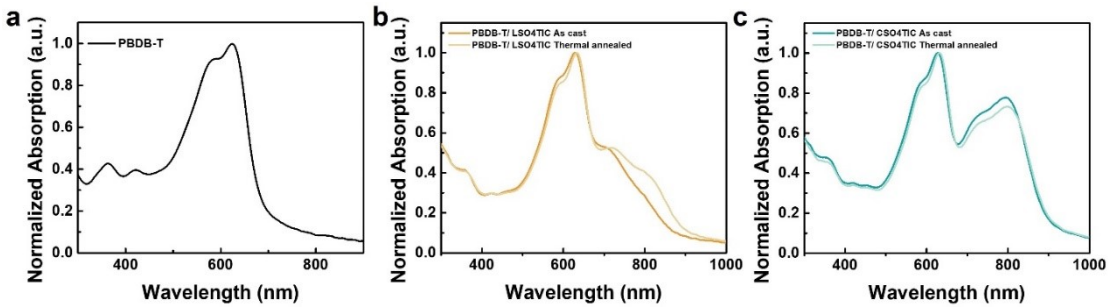

Figure S9. The UV-Vis spectra of **a)** PBDB-T pure film and **b-c)** PBDB-T/ CSO4TIC and PBDB-T/ LSO4TIC films.

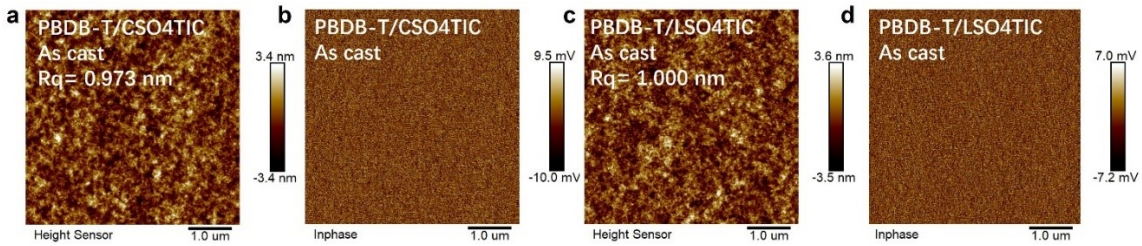

Figure S10. AFM **a, c)** height images and **b, d)** phase images of pristine PBDB-T/ CSO4TIC and PBDB-T/ LSO4TIC films.

Table S1. Summary of the molecular packing structure of non-fused ring acceptors.

Non-fused ring acceptors with lamellar packing structures		
Acceptor	**Molecular packing**	**Ref.**
CH3−2F	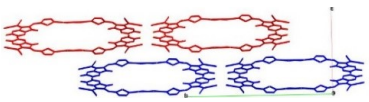	**2**
PTB4Cl	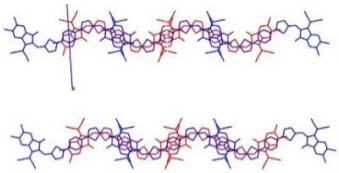	**3**
PTB4F	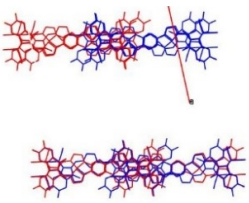	

A4T-25	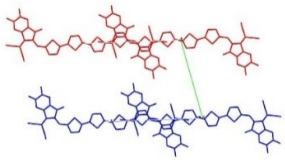	**4**
A4T-26	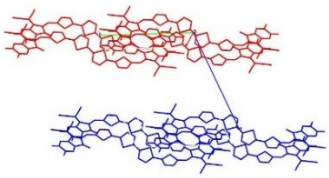	
2T2Se-F	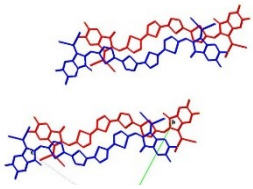	**5**
BO-4T	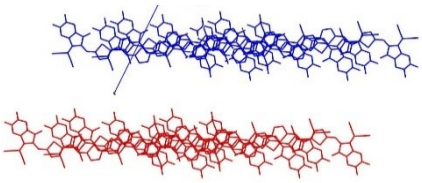	**6**
LSO4TIC	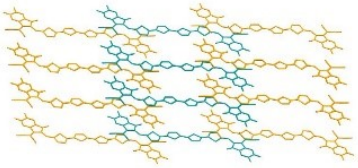	**This work**
Non-fused ring acceptors with 3D network packing structures		
Acceptor	**Molecular packing**	**Ref.**
2BTh-2F	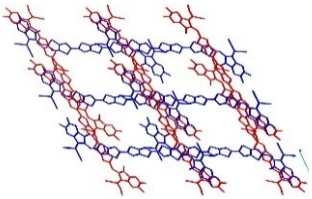	**7**
A4T-16	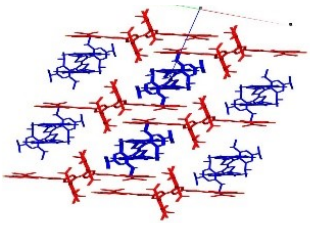	**8**

L1	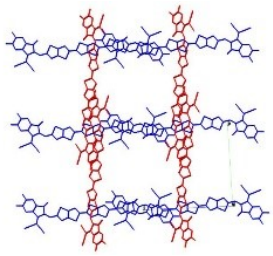	**9**
L2	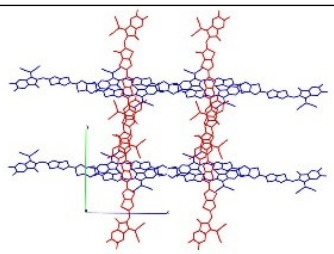	
CSO4TIC	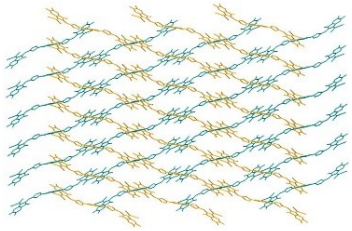	**This work**

Table S2. Reorganization energies (4 Point Method).

Molecules	**λ_1 (meV)**	**λ_2 (meV)**	**λ_3 (meV)**
LSO4TIC-hole	109.36	106.99	216.35
LSO4TIC-electron	97.33	85.06	182.39
CSO4TIC -hole	105.17	103.08	208.25
CSO4TIC -electron	100.51	88.48	188.99

Table S3. Mobilities simulated by the Monte Carlo method with quantum dynamics.

Molecules	**μ_a ($cm^2\ V^{-1}\ s^{-1}$)**	**μ_b ($cm^2\ V^{-1}\ s^{-1}$)**	**μ_c ($cm^2\ V^{-1}\ s^{-1}$)**	**μ ($cm^2\ V^{-1}\ s^{-1}$)**

LSO4TIC-hole	0.0068	0.0061	0.0011	0.0044
LSO4TIC-electron	0.0005	0.0079	0.0014	0.0030
CSO4TIC-hole	0.0216	0.1292	0.0465	0.0675
CSO4TIC-electron	0.1969	1.5165	0.0258	0.5793

Table S4. Crystal data and structure refinement for LSO4TIC and CSO4TIC.

	LSO4TIC	**CSO4TIC**
CCDC number	2277927	2277928
Empirical formula	$C_{82}H_{78}F_4N_4O_6S_4$	$C_{82}H_{74}F_4N_4O_6S_4$
Formula weight	1419.72	1415.69
Temperature [K]	193.00	193.00
Crystal system	triclinic	monoclinic
Space group (number)	$P\bar{1}$ (2)	$P2_1/c$ (14)
a [Å]	7.3494(2)	8.1524(2)
b [Å]	19.2273(5)	22.8699(6)
c [Å]	20.6995(6)	23.8167(7)
α [°]	63.4650(10)	90
β [°]	81.3270(10)	99.6740(10)
γ [°]	81.9660(10)	90
V [Å^3]	2578.31(12)	4377.3(2)
Z	1	2
ρ_{calc} [g cm^{-3}]	0.914	1.074
μ [mm^{-1}]	0.806	0.949
2θ range [°]	7.57 to 108.06 (0.83 Å)	4.69 to 120.58 (0.77 Å)
Data / Restraints / Parameters	9405/ 115/ 484	9533/ 173/ 489
Goodness-of-fit on F^2	1.088	0.951
Final R indexes	R_1 = 0.0918	R_1 = 0.0959
[$I \geq 2\sigma(I)$]	wR_2 = 0.2703	wR_2 = 0.2579
Final R indexes	R_1 = 0.1086	R_1 = 0.1163

[all data]	wR_2 = 0.2832	wR_2 = 0.2774
Largest peak/ hole [eÅ^{-3}]	0.65/ -0.58	1.52/ -0.72

Table S5. Photovoltaic parameters of the CSO4TIC devices with different polymer donors.

Active layer	V_{oc} (V)	J_{sc} (mA cm^2)	FF (%)	PCE (%)
PM6/ CSO4TIC	0.89	15.50	42.07	5.79
D18/ CSO4TIC	0.90	15.74	58.91	8.31

Table S6. The photovoltaic performance of PBDB-T/ CSO4TIC based devices with different donor concentrations (0.75% 1-chloronaphthalene added) under the illumination of AM 1.5G.

Active layer	Donor conc. (mg/ mL)	V_{oc} (V)	J_{sc} (mA cm^2)	FF (%)	PCE (%)
PBDB-T/ CSO4TIC	8	0.83	21.54	65.40	11.70
	9	0.83	23.18	64.08	12.35
	10	0.83	24.78	62.76	12.84
	11	0.83	24.81	60.32	12.36
	12	0.82	24.22	53.93	10.69

Table S7. The photovoltaic performance of PBDB-T/ CSO4TIC based devices with different acceptor concentrations (0.75% 1-chloronaphthalene added) under the illumination of AM 1.5G.

Active layer	Acceptor conc. (mg/ mL)	V_{oc} (V)	J_{sc} (mA cm^2)	FF (%)	PCE (%)
PBDB-T/ CSO4TIC	4	0.80	23.55	55.06	10.41
	6	0.80	26.16	62.78	13.19
	8	0.81	25.59	61.67	12.75

Table S8. The photovoltaic performance of **PBDB-T/ CSO4TIC** based devices with

different solid additive concentrations (DBCl) under the illumination of AM 1.5G.

Active layer	Additive conc. (mg/ mL)	V_{oc} (V)	J_{sc} (mA cm^2)	FF (%)	PCE (%)
PBDB-T/ CSO4TIC	8	0.81	25.91	65.51	13.80
	10	0.81	26.15	65.60	13.95
	12	0.81	25.58	65.82	13.57

Table S9. The average photovoltaic performance of PBDB-T/ CSO4TIC based devices (10 mg/ mL DBCl added) with different annealing temperatures for 10 min.

Active layer	Annealing temp. (°C)	V_{oc} (V)	J_{sc} (mA cm^2)	FF (%)	PCE (%)
PBDB-T/ CSO4TIC	80	0.82	24.48	65.00	12.99
	100	0.82	24.58	65.79	13.18
	120	0.82	24.63	66.11	13.29

Table S10. The photovoltaic performance of PBDB-T/ CSO4TIC based devices (10 mg/ mL DBCl added) with 120°C thermal annealing for different annealing times.

Active layer	Annealing times (min)	V_{oc} (V)	J_{sc} (mA cm^2)	FF (%)	PCE (%)
PBDB-T/ CSO4TIC	10	0.81	26.00	66.82	14.09
	15	0.81	26.00	67.52	14.22
	20	0.81	25.79	67.21	13.96

Table S11. The photovoltaic performance of PBDB-T/ LSO4TIC based devices with different solid additive concentrations (2-IN) under the illumination of AM 1.5G.

Active layer	Additive conc. (mg/ mL)	V_{oc} (V)	J_{sc} (mA cm^2)	FF (%)	PCE (%)
PBDB-T/ LSO4TIC	5	0.85	21.89	53.19	9.93
	10	0.85	23.86	62.31	12.64
	15	0.84	22.97	64.55	12.41

Table S12. The photovoltaic performance of PBDB-T/ LSO4TIC based devices (10 mg/ mL 2-IN added) with different annealing temperatures for 10 min.

Active layer	Annealing temp. (°C)	V_{oc} (V)	J_{sc} (mA cm^2)	FF (%)	PCE (%)
PBDB-T/ LSO4TIC	100	0.85	23.70	57.94	11.61
	120	0.84	23.67	62.35	12.46
	140	0.84	23.65	60.72	12.07

Table S13. The photovoltaic performance of PBDB-T/ LSO4TIC based devices (10 mg/ mL 2-IN added) with 120°C thermal annealing for different annealing times.

Active layer	Annealing times (min)	V_{oc} (V)	J_{sc} (mA cm^2)	FF (%)	PCE (%)
PBDB-T/ LSO4TIC	2	0.86	22.12	54.92	10.43
	5	0.85	23.87	62.17	12.56
	10	0.84	23.45	60.84	11.92

Table S14. Energy loss values for the PBDB-T/ LSO4TIC and PBDB-T/ CSO4TIC-Based Devices.

Active layers	E_g (eV)	E_{loss} (eV)	ΔE_1 (eV)	ΔE_2 (eV)	ΔE_3 (eV)	V_{oc}^{sq} (V)	V_{oc}^{rad} (V)	EQE_{EL} (%)	$\Delta E_{non\text{-}rad}$ (eV)
PBDB-T/ LSO4TIC	1.448	0.602	0.265	0.069	0.269	1.183	1.115	5.34E-05	0.253
PBDB-T/ CSO4TIC	1.422	0.621	0.263	0.058	0.300	1.159	1.101	6.24E-05	0.249

4. ^{1}H NMR Spectra

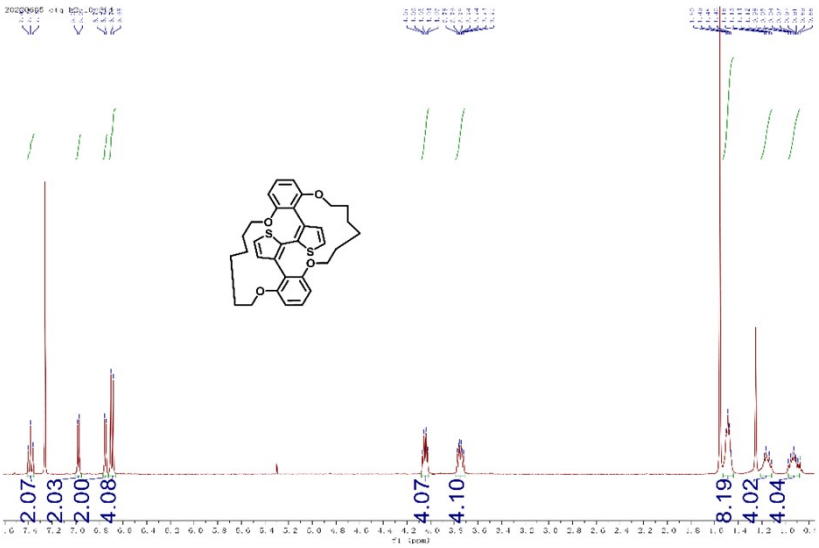

Figure S11. ^{1}H NMR spectrum of compound **1** in $CDCl_3$ at 400 MHz.

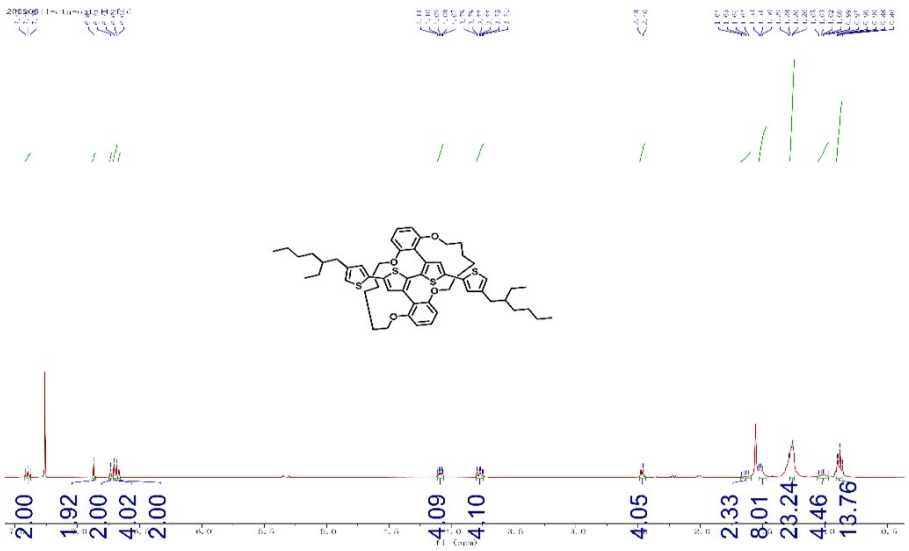

Figure S12. ^{1}H NMR spectrum of compound **3** in $CDCl_3$ at 400 MHz.

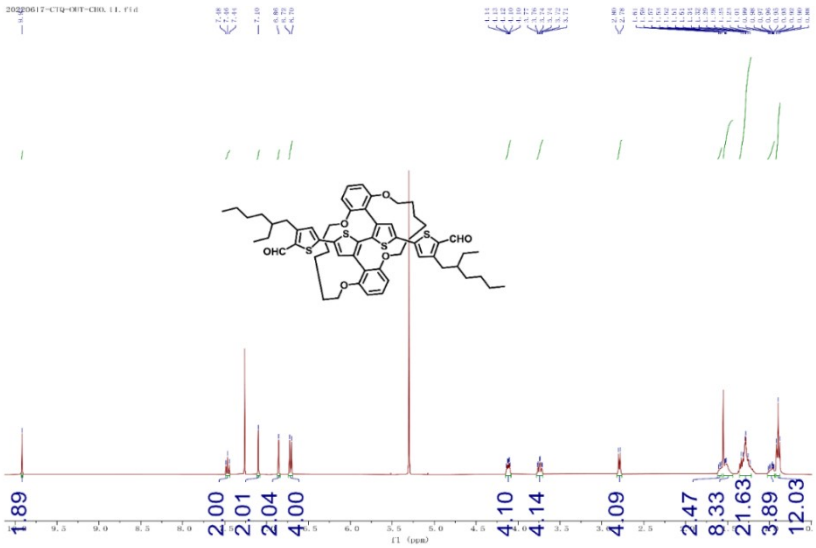

Figure S13. ^{1}H NMR spectrum of compound **4** in $CDCl_3$ at 400 MHz.

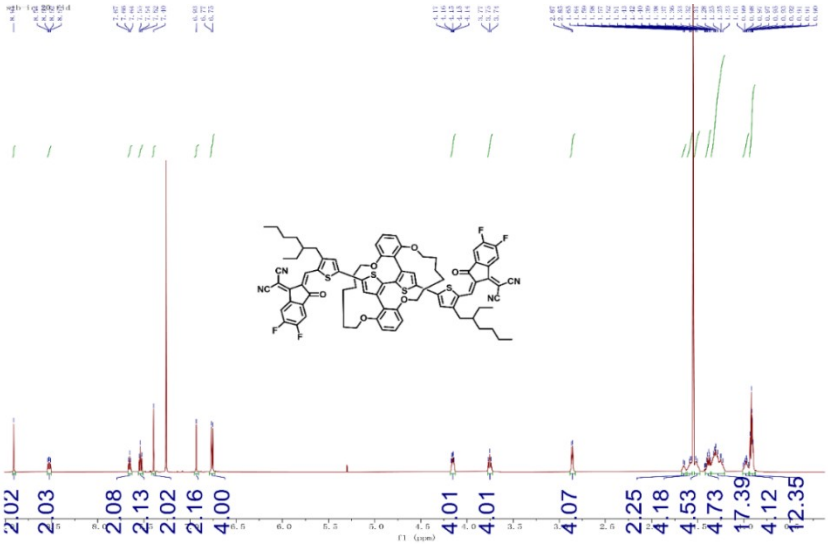

Figure S14. ^{1}H NMR spectrum of **CSO4TIC** in $CDCl_3$ at 600 MHz.

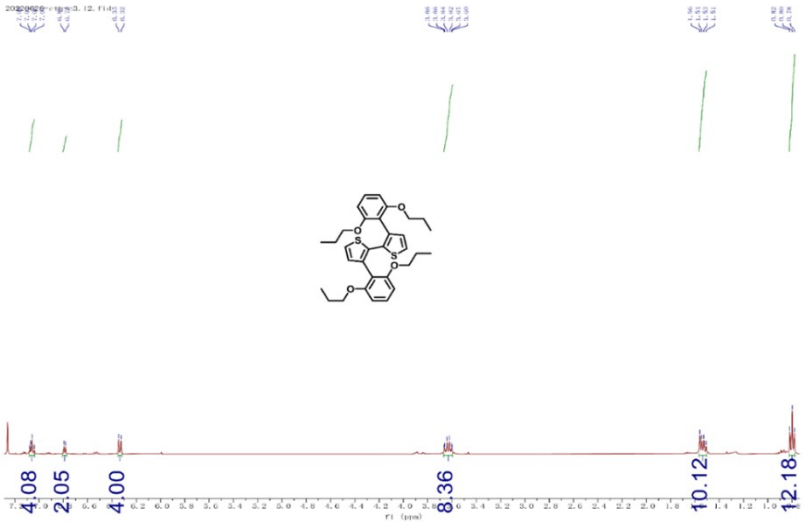

Figure S15. ^{1}H NMR spectrum of compound **5** in $CDCl_3$ at 400 MHz.

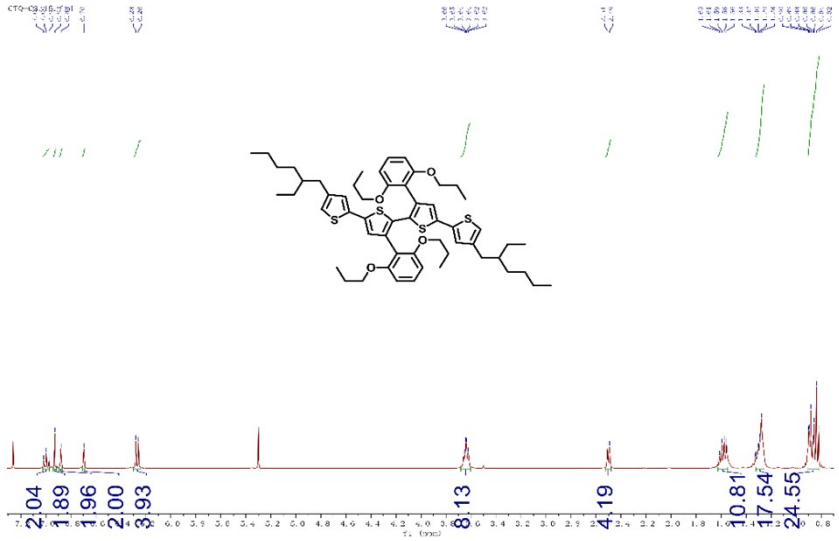

Figure S16. ^{1}H NMR spectrum of compound **7** in $CDCl_3$ at 400 MHz.

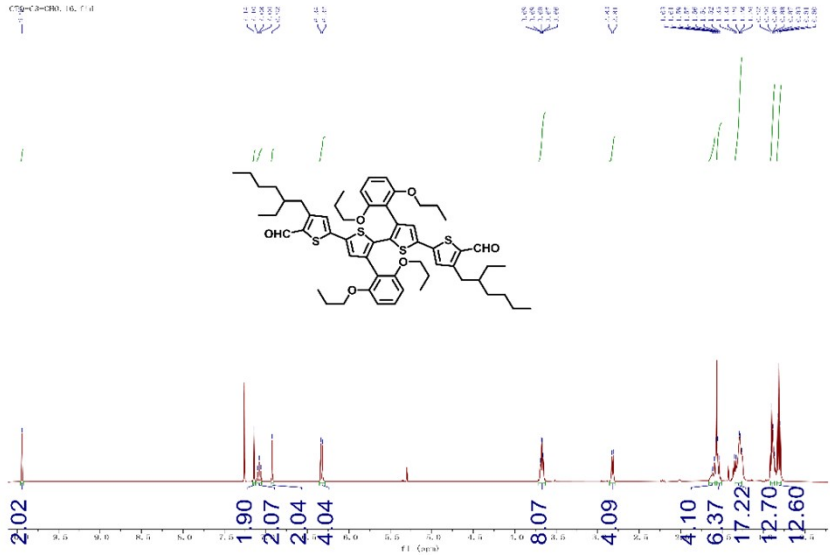

Figure S17. ^{1}H NMR spectrum of compound **8** in $CDCl_3$ at 400 MHz.

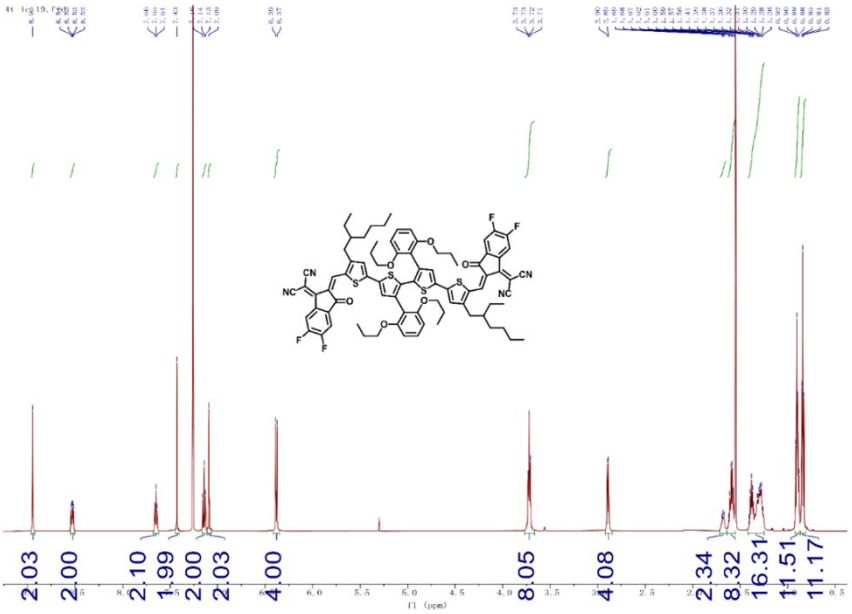

Figure S18. ^{1}H NMR spectrum of **LSO4TIC** in $CDCl_3$ at 600 MHz.

5. MALDI-TOF MS Spectra

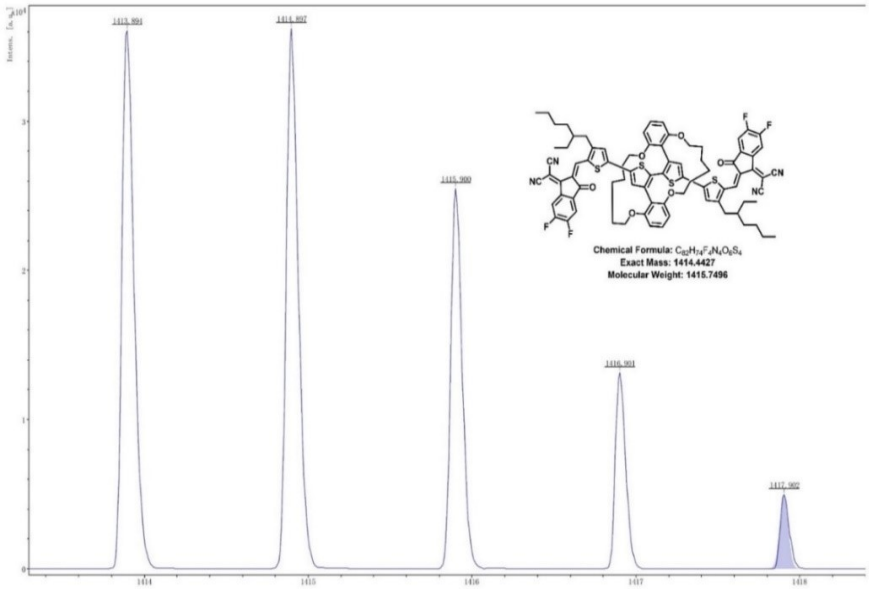

Figure S19. MS (MALDI-TOF) spectrum of **CSO4TIC**.

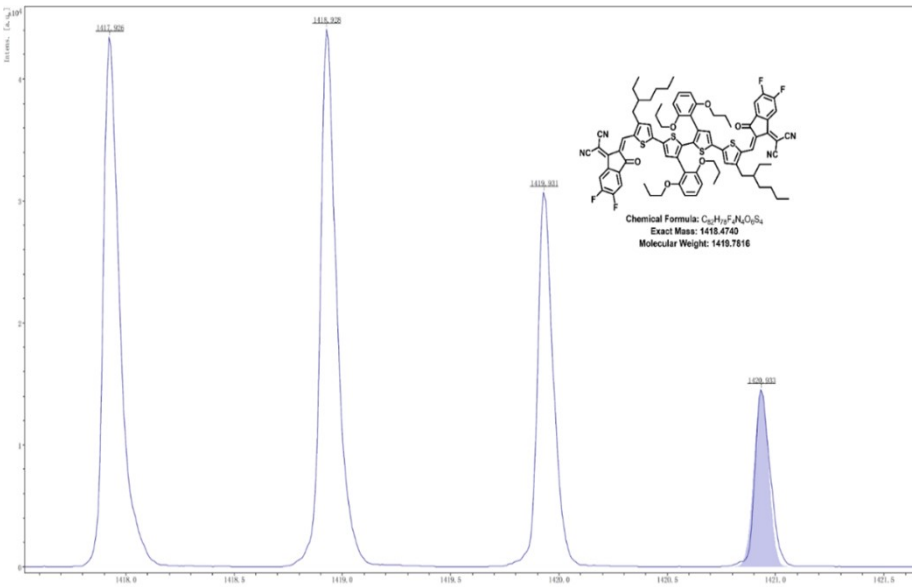

Figure S20. MS (MALDI-TOF) spectrum of **LSO4TIC**.

6. References

1. K. Sugiyasu, Y. Honsho, R. M. Harrison, A. Sato, T. Yasuda, S. Seki and M. Takeuchi, *J. Am. Chem. Soc.*, 2010, **132**, 14754-14756.
2. X. Wang, H. Lu, J. Zhou, X. Xu, C. e. Zhang, H. Huang, J. Song, Y. Liu, X. Xu, Z. Xie, Z. Tang and Z. Bo, *ACS Appl. Mater. Interfaces*, 2021, **13**, 39652-39659.
3. T.-J. Wen, Z.-X. Liu, Z. Chen, J. Zhou, Z. Shen, Y. Xiao, X. Lu, Z. Xie, H. Zhu, C.-Z. Li and H. Chen, *Angew. Chem. Int. Ed.*, 2021, **60**, 12964-12970.
4. J. Li, H. Li, L. Ma, Y. Xu, Y. Cui, J. Wang, J. Ren, J. Zhu, S. Zhang and J. Hou, *Small Methods*, 2022, **6**, 2200007.
5. X. Ding, X. Chen, Y. Xu, Z. Ni, T. He, H. Qiu, C.-Z. Li and Q. Zhang, *Chem. Eng. J.*, 2022, **429**, 132298.
6. Q. Shen, C. He, S. Li, L. Zuo, M. Shi and H. Chen, *J. Mater. Chem. A*, 2023, **11**, 3575-3583.
7. X. Wang, H. Lu, Y. Liu, A. Zhang, N. Yu, H. Wang, S. Li, Y. Zhou, X. Xu, Z. Tang and Z. Bo, *Adv. Energy Mater.*, 2021, **11**, 2102591.
8. L. Ma, S. Zhang, J. Zhu, J. Wang, J. Ren, J. Zhang and J. Hou, *Nat. Commun.*, 2021, **12**, 5093.
9. D.-L. Ma, Q.-Q. Zhang and C.-Z. Li, *Angew. Chem. Int. Ed.*, 2023, **62**, e202214931.